The Goddard Coastal Wave Model. Part II: Kinematics

RAY Q. LIN AND NORDEN E. HUANG

Laboratory for Oceans, NASA/Goddard Space Flight Center, Greenbelt, Maryland

(Manuscript received 12 January 1994, in final form 9 May 1995)

ABSTRACT

A new coastal wave model is being developed to study air–sea interaction processes in the coastal region. The kinematics of this model, which govern the wave propagation, are reported. This new model is based on the action conservation equation rather than on the energy transport equation; it also employs the full nonlinear dispersion relationship in water of arbitrary depth. With these improvements, it includes nonstationary wave–current interaction processes and functions in coastal regions with variable finite water depths. Numerical results show that these changes cause significant differences between the new model and the WAM model when waves encounter any steady or unsteady current, and when waves propagate over changing bottom topography in a shallow water region. Such conditions are very common and should not be neglected in the coastal regions.

1. Introduction

To test the validity of any numerical model, one should examine the following areas: the numerics, the kinematics, and the dynamics. Each element is critical to the final result; clearly, their effects should be determined separately. Numerics address the numerical schemes, while kinematics address the rule of wave propagation. In water wave studies, the kinematics, or the dispersion relationship, assumes a far more important role than simply governing the motion of the waves; it is also the key in determining certain critical dynamical processes. For example, the resonance condition in weakly nonlinear wave–wave interactions is determined by the dispersion relationship.

The problems of numerics have been discussed in Part I (Lin and Huang 1996, hereafter referred to as Part I) of this paper series. In that paper, we have shown that the group velocity appears in two of the parameters that determines the computational dispersion. The first is the computational dispersion parameter defined as

$$(c_g + u)^*/(c_g + u), \tag{1}$$

where $(c_g + u)^*$ is the computational velocity and $(c_g + u)$ is the true physical group velocity plus the ambient current velocity. In order to obtain $(c_g + u)^*$, we also have to introduce a computational phase error θ^*, defined as

$$-\theta^* = \tan^{-1}(-\Lambda_i/\Lambda_r), \tag{2}$$

where Λ is the computational stability parameter, Λ_i is the imaginary part, and Λ_r is the real part of Λ.

The second important computational parameter is the nondimensional grid size, defined as

$$\mu_j = (c_g + u)_j \Delta t/\Delta x \tag{3}$$

in which Δt is the time step, Δx is the grid size, and $(c_g + u)_j$ is the velocity at gridpoint j. These parameters appeared in many of the analytic expressions of the computation analysis discussed in Part I.

In addition to computational needs, the dispersion relationship is central to many nonlinear wave phenomena. Therefore, the correct kinematics is essential to the numerical scheme. In this paper, we will focus on the kinematics problem for the coastal region, where not only nonlinearity, but also the complications of bottom topographic features and tidal currents, will all have notable effects on the kinematics. We found that previous models invoked many inadequate assumptions. For example, the subtle assumption of conservation of wavenumber must be modified to accommodate the changing bottom topography and the presence of variable currents. Also, strict adherence to the linear dispersion relationship should be abandoned in order to be logically consistent in studying nonlinear wave–wave interactions.

In the following sections, we will describe the kinematics of the Goddard Coastal Wave Model (GCWAM), which will include the modifications we deemed important. The results will be compared with the state-of-the-art WAM model (Günther et al. 1993) whenever possible. But before comparing the models, we will first present the major kinematic differences between the GCWAM and the latest version of the WAM model.

Corresponding author address: Dr. Ray-Qing Lin, Code 5030, David Taylor Model Basin, Carderock Division, NSWC, Bethesda, MD 20084-5000.

2. The dispersion relationship used in GCWAM

It is well known that for nonlinear water waves, the dispersion relation will be weakly amplitude dependent. Although the effects of the nonlinearity are usually small in wave propagation, the need for a full nonlinear dispersion relation has been made amply clear by numerous papers on the nonlinear wave evolution (see, for example, Yuen and Lake 1982; Infeld and Rowlands 1990). There we can see that the nonlinear dispersion relationship is not only a factor in governing the modulation and propagation of the waves, but also a key in modifying the resonant interaction conditions as reported by McLean (1982). Therefore, it is not only logically imperative but also intellectually satisfying to adopt such a fuller dispersion relationship. For these reasons, we decided to adopt the full nonlinear dispersion, as given in Whitham (1974), to examine its effects. Following Whitham, we have

$$\sigma = \left\{(gk\tanh kd)\left[1 + \left(\frac{9\tanh^4 kd - 10\tanh^2 kd + 9}{8\tanh^4 kd}\right)k^2a^2 + \cdots\right]\right\}^{1/2}, \quad (4)$$

in which σ is the intrinsic frequency in radians per second; $(\vec{\ })$ is vector, k is the magnitude of the vector wavenumber $\vec{k}$ in per meter; g is gravitational acceleration (m s^{-2}); d is the depth (m); and a is the amplitude of the wave.

By definition,

$$\vec{c}_g = \frac{\partial\sigma}{\partial k}\frac{\vec{k}}{k}, \quad \vec{C} = \frac{\omega}{k}\frac{\vec{k}}{k}, \quad \text{and} \quad \vec{c} = \frac{\sigma}{k}\frac{\vec{k}}{k}, \quad (5)$$

where $\vec{c}_g$ is the intrinsic group velocity; ω is the apparent frequency defined as $\omega = \sigma + \vec{k}\cdot\vec{V}$ with $\vec{V}$ as the ambient current in meters per second, and $\vec{C}$ and $\vec{c}$ are the apparent and intrinsic phase velocity respectively. In terms of the spectral representation, the full nonlinear group velocity should be

$$\vec{c}_g = \left\{0.5\left[\frac{g}{k}\tanh kd\right]^{1/2}\left[1 + \frac{2kd}{\sinh(2kd)}\right][1 + f_{p(k,d)}k^2\mathrm{N}]^{1/2}\right\}\frac{\vec{k}}{k} + \left\{0.5\frac{(gk\tanh kd)^{1/2}}{[1 + f_{p(k,d)}k^2\mathrm{N}]^{1/2}}\left[\left(\frac{\partial\mathrm{N}}{\partial k}k^2 + 2k\mathrm{N}\right)f_{p(k,d)} + k^2 d\mathrm{N}df_{p(k,d)}\right]\right\}\frac{\vec{k}}{k}, \quad (6)$$

in which N is density energy spectrum, and $f_{p(k,d)}$ and $df_{p(k,d)}$ are given as follows:

$$f_{p(k,d)} = \frac{9}{8} - \frac{10}{8\tanh^2 kd} + \frac{9}{8\tanh^4 kd}, \quad (7)$$

$$df_{p(k,d)} = \frac{10\,\mathrm{sech}^2 kd}{4\tanh^3 kd} - \frac{9\,\mathrm{sech}^2 kd}{2\tanh^5 kd}. \quad (8)$$

It should be noted that when we consider the presence of time varying tidal currents, not only a, but also d, are functions of position and time. With the introduction of the position-dependent amplitude and depth in the nonlinear dispersion relationship, the wavenumber can no longer be assumed to be conserved automatically. Rather, we should have

$$\sigma = W[k(x,t), d(x,t), a(x,t)]; \quad (9)$$

therefore, following the group velocity, we have

$$\frac{Dk_i}{Dt} = -\frac{\partial W}{\partial d}\frac{\partial d}{\partial x_i} - \frac{\partial W}{\partial a}\frac{\partial a}{\partial x_i}, \quad (10)$$

with $D(\ )/Dt$ the material derivative following the wave group. Here, we have considered the variations of both the amplitude and the depth, and assumed that they are of the same order of magnitude. These variations of wavenumber and frequency have been neglected by all previous modelers, but they have been clearly pointed out as important considerations in the nonlinear wave evolution process by Whitham (1974) in a discussion of wave kinematics. They should thus be included in the coastal wave model.

Now, the basic equation for the GCWAM model is

$$\frac{\partial\mathrm{A}}{\partial t} + \frac{\partial[c_{g\lambda}\mathrm{A}]}{\partial\lambda} + \cos\phi^{-1}\frac{\partial[c_{g\phi}\cos\phi\mathrm{A}]}{\partial\phi} + \frac{\partial[c_\theta\mathrm{A}]}{\partial\theta} + \frac{\partial[c_\omega\mathrm{A}]}{\partial\omega} = S, \quad (11)$$

in which A (m^2/Hz^2) is the action density spectrum defined as the energy spectrum divided by the intrinsic frequency σ, a generalized definition of action for a single train of waves (Bretherton and Garrett 1968); t is the time (s); ϕ and λ are the latitude and longitude coordinates, respectively; θ is the propagation angle (when $\theta = 0$, the direction is from the south while the direction rotates clockwise as θ increases); and S is the

energy source term. In this study, we again assume $S = 0$ in order to examine the kinematic problem separately.

Equation (11) is very different from the one used in WAM. The WAMDI Group (1988) used an equation for the conservation of energy in a form similar to Eq. (11), but it was designated as "the transport equation" for a subtle reason: they had designed the model for deep water and without variable currents. Therefore, both frequency and group velocity would be invariant as far as position is concerned. Then, the group velocity can be moved outside of the gradient operator. Under that condition, even the difference between the action density and energy density is a constant ratio independent of position. Consequently, in the actual WAM program, the equation used is essentially

$$\frac{DN}{Dt} = \frac{\partial N}{\partial t} + c_{g\lambda}\frac{\partial N}{\partial \lambda} + \cos\phi^{-1} c_{g\phi}\frac{\partial N}{\partial \phi} + c_\theta \frac{\partial N}{\partial \theta} = S, \tag{12}$$

in which N (m^2/Hz) is the energy density spectrum.

From (12), one can see that in the WAM, the energy is an invariant following a wave when the source functions are set to zero. Changes in the energy density must come from the source functions. In the deep ocean this may be an acceptable approximation, but in coastal waters it is grossly in error. Even under steady conditions and without any ambient currents, the bottom topography will cause the energy density to change. With the WAM we cannot even recover the simple analytic result derived for a wave propagating toward the beach under steady-state conditions without currents, as given by Phillips (1977):

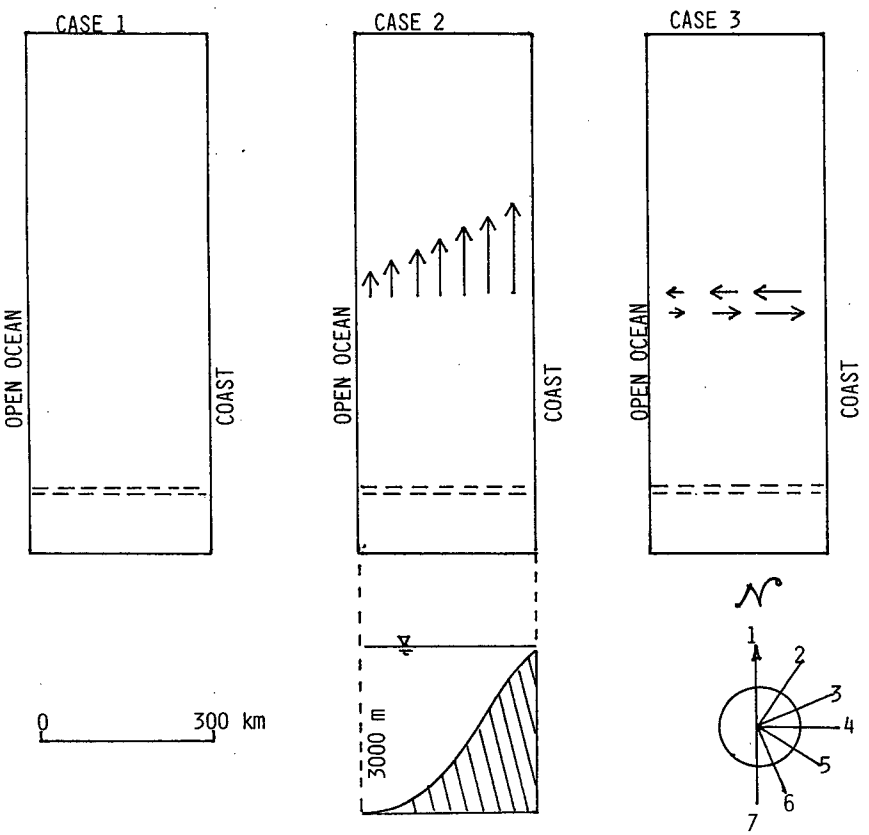

FIG. 1. A schematic view of the coastal test conditions. The test region is a box 300 km × 900 km with the coastline running in the north–south direction, and the coastline located on the east side. The depth at the open ocean side is nominally 3000 m and at the coastline is 2.5 m. Test results are computed along the dashed line located 100 km from the southern boundary. Wave direction is indicated by the numbers shown at the right lower corner. The swell spectrum used in all the numerical tests is the same as that given in Part I. The test conditions for the three coastal cases are as follows. Case 1: coastal region with no current, case 2: coastal region with a steady shear current with magnitude increasing from 0.2 m s^{-1} at the open ocean side to 1.0 m s^{-1} at the coastline, and case 3: coastal region with an on–offshore tidal current with magnitude increasing from 0.2 m s^{-1} at the open ocean side to 1.0 m s^{-1} at the coastline.

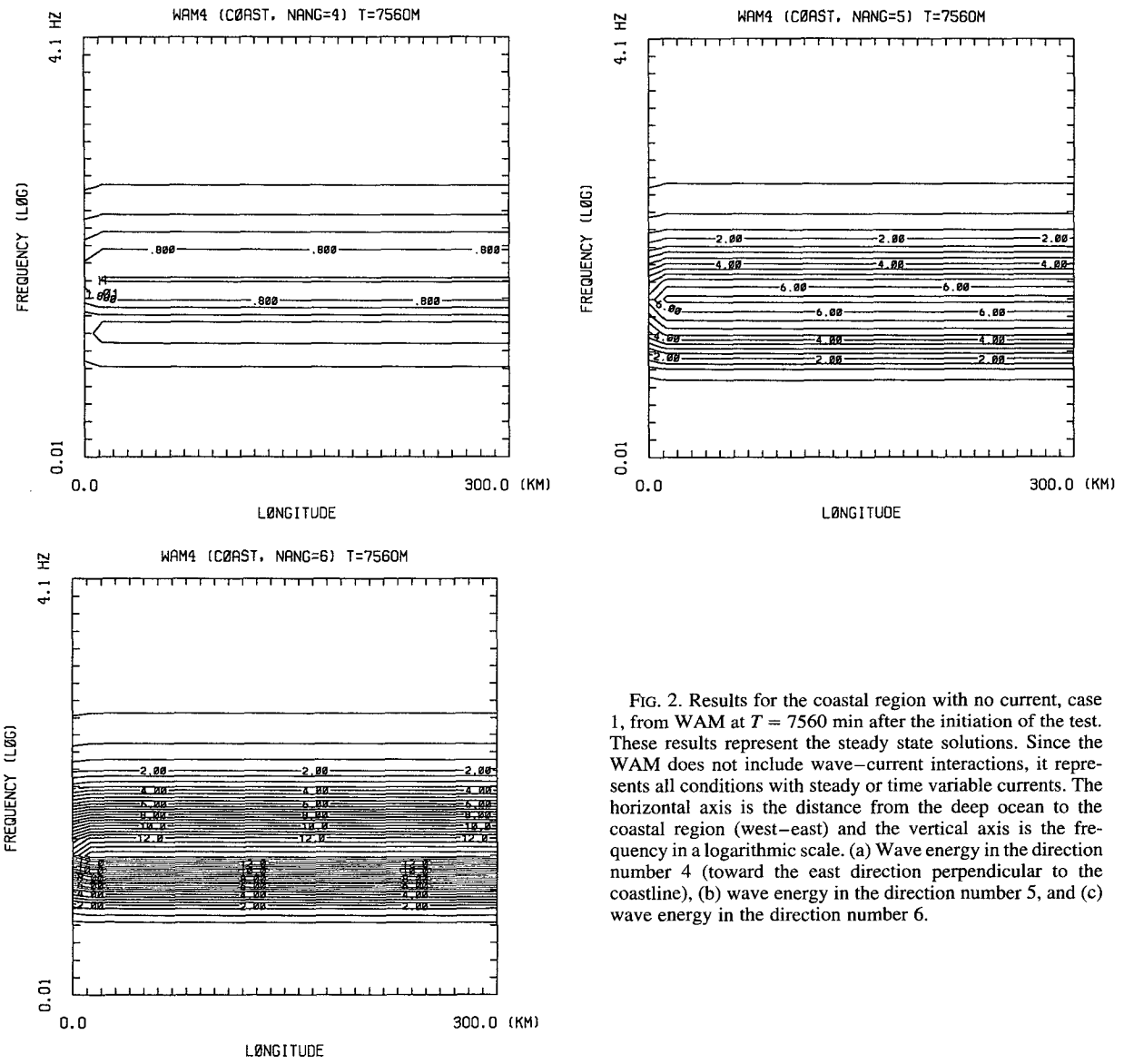

FIG. 2. Results for the coastal region with no current, case 1, from WAM at $T = 7560$ min after the initiation of the test. These results represent the steady state solutions. Since the WAM does not include wave–current interactions, it represents all conditions with steady or time variable currents. The horizontal axis is the distance from the deep ocean to the coastal region (west–east) and the vertical axis is the frequency in a logarithmic scale. (a) Wave energy in the direction number 4 (toward the east direction perpendicular to the coastline), (b) wave energy in the direction number 5, and (c) wave energy in the direction number 6.

$$N c_g = \text{const.}$$

It should be pointed that the conservation of either the energy or the action density does not require constancy of either energy or action density; only that the energy flux should be constant.

The insignificant difference between GCWAM and WAM in deep water without ambient currents becomes a major issue in the coastal region, where tidal currents and changing topography will both make the group velocity and even the intrinsic frequency a function of position. Indeed, these effects do make substantial differences in the model results as will be shown later through more detailed model results.

To consider the full variations of group velocity in the numerical computations, we also have to derive expressions for the transport velocities, $c_{g\lambda}$, $c_{g\phi}$, c_θ, and c_ω, which are given by the following expressions:

$$c_{g\lambda} = \frac{D\lambda}{Dt} = \frac{c_g \sin\theta + u}{R\cos\phi}, \tag{13}$$

$$c_{g\phi} = \frac{D\phi}{Dt} = \frac{c_g \cos\theta + v}{R}, \tag{14}$$

$$c_\theta = \frac{D\theta}{Dt} = \frac{c_g \tan\phi \sin\theta}{R} + \frac{\partial \vec{C}}{\partial \mathbf{n}}, \tag{15}$$

$$c_\omega = \frac{D\omega}{Dt} \tag{16}$$

in which R is the radius of the earth, and $\mathbf{n}$ is the unit vector in the tangential direction to $\vec{C}$. Of the four trans-

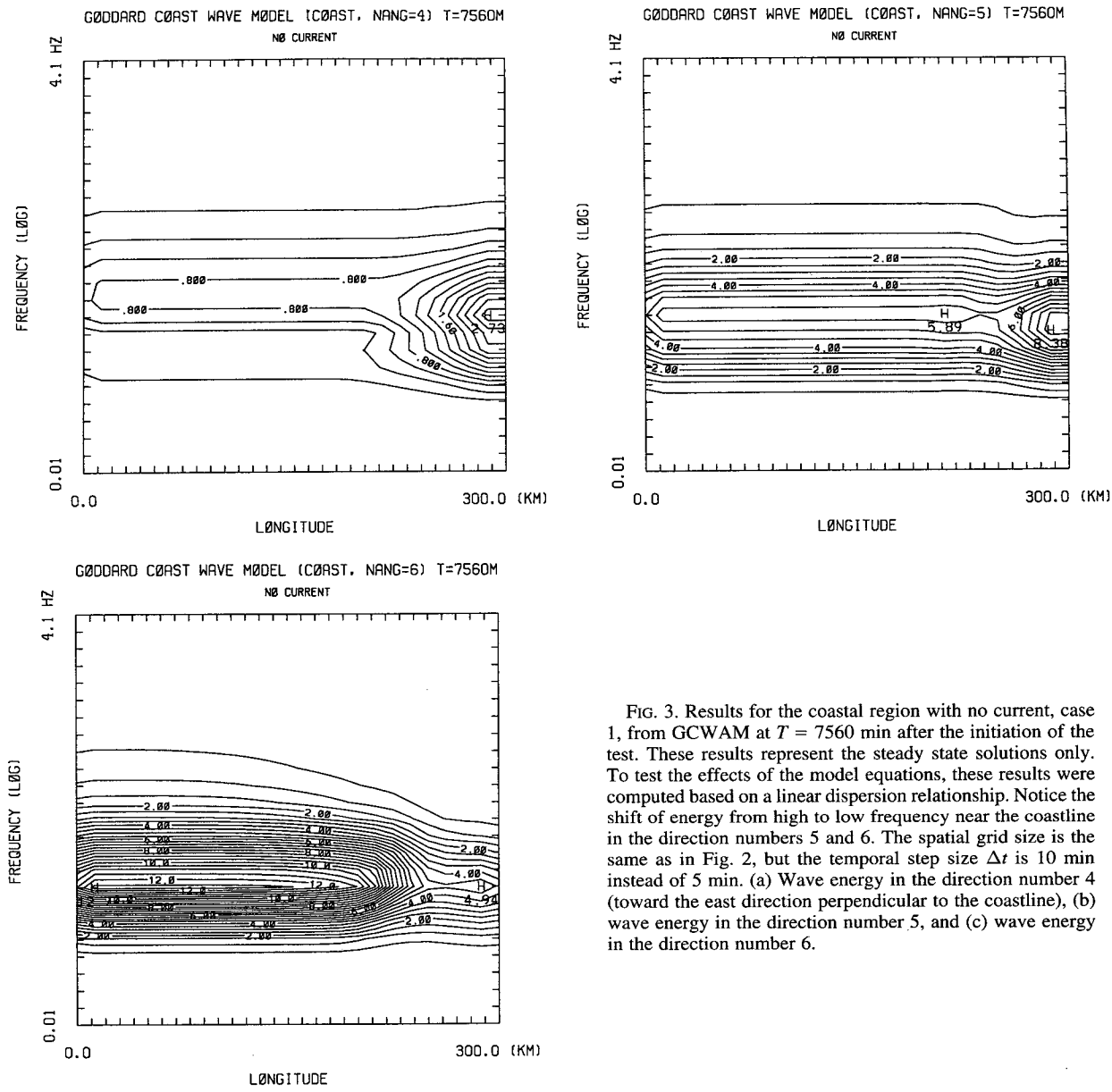

FIG. 3. Results for the coastal region with no current, case 1, from GCWAM at $T = 7560$ min after the initiation of the test. These results represent the steady state solutions only. To test the effects of the model equations, these results were computed based on a linear dispersion relationship. Notice the shift of energy from high to low frequency near the coastline in the direction numbers 5 and 6. The spatial grid size is the same as in Fig. 2, but the temporal step size Δt is 10 min instead of 5 min. (a) Wave energy in the direction number 4 (toward the east direction perpendicular to the coastline), (b) wave energy in the direction number 5, and (c) wave energy in the direction number 6.

port velocities, the first three are included in WAM (1988). Though the fourth transport velocity, c_ω, is not included in WAM, it has been included in Tolman (1991). It was, however, neglected by Tolman (1992) when the model was used in deep water. Such an omission is unacceptable if the model is to be used for anything other than a linear homogeneous wave field in deep water. Mathematically, Eqs. (15) and (16) may be written as

$$c_\theta = \frac{1}{k}\frac{\partial \sigma}{\partial d}\frac{\partial d}{\partial n} + \frac{1}{k}(c_g - c)\frac{\partial k}{\partial n} + \frac{\vec{k}}{k}\cdot\frac{\partial \vec{V}}{\partial n}; \quad (17)$$

$$c_\omega = \frac{D\omega}{Dt} = \frac{\partial(\sigma + \vec{k}\cdot\vec{V})}{\partial t} + (\vec{c}_g + \vec{V})\cdot\nabla(\sigma + \vec{k}\cdot\vec{V}). \quad (18)$$

It is clear that, even under steady-state conditions, $c_\omega \neq 0$, if there is spatial gradient of the apparent frequency. The contribution to c_ω can come from temporal variations as well as spatial modulation of waves through variations of the currents and bottom topographic features. Because of the time-varying currents and nonuniform water depth in the coastal region, the dispersion relationship is more complicated. It should not be simplified as in the WAM model for coastal applications.

3. Results

Having established the analytic expressions for the kinematics, we will present some numerical results to

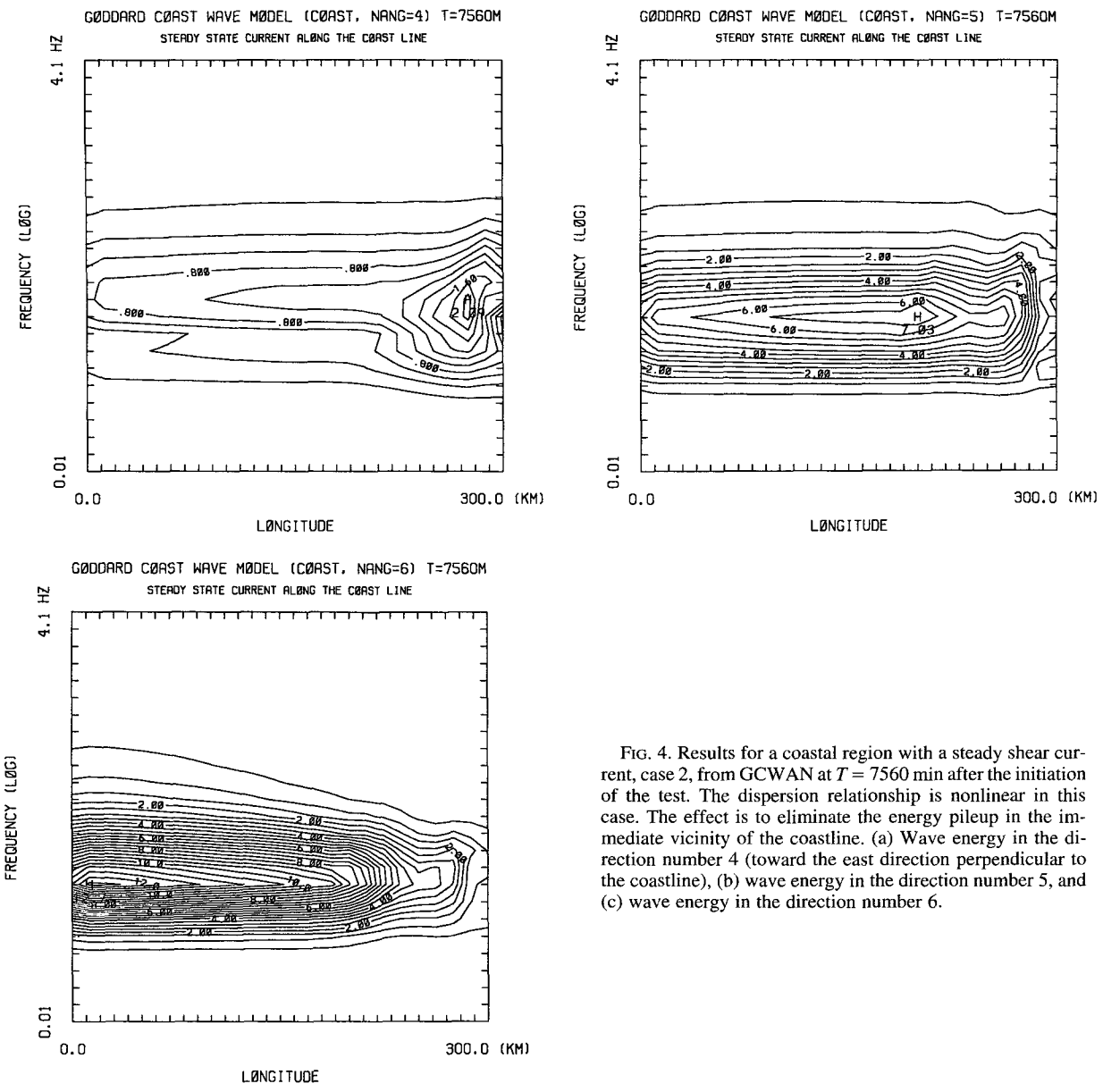

FIG. 4. Results for a coastal region with a steady shear current, case 2, from GCWAN at $T = 7560$ min after the initiation of the test. The dispersion relationship is nonlinear in this case. The effect is to eliminate the energy pileup in the immediate vicinity of the coastline. (a) Wave energy in the direction number 4 (toward the east direction perpendicular to the coastline), (b) wave energy in the direction number 5, and (c) wave energy in the direction number 6.

illustrate the differences between the full nonlinear dispersion relation used in the GCWAM and the linear approximations used in the WAM. Of course, in most of the comparisons we cannot totally exclude the influences of the different numerical schemes and different types of model equations, for the WAM uses the transport equation, whereas we use the action conservation equation with a full nonlinear dispersion relationship. We will try to illustrate the effects of nonlinearity and types of equations as far as possible.

Two types of test sites are selected for the study: a coastal region and an open ocean region over a seamount. In the coastal region, we want to see the variations of the sea state due to effects of bottom topography and time-varying tidal currents. To eliminate other complications, the tests are designed to study the propagation of waves over an infinitely long uniform coastline. Therefore, the tests are conducted in an idealized coastal region with bottom topography. The test conditions are summarized schematically in Fig. 1. The area is 300 by 900 km with the depth changing from 2995 m in the open ocean to 2.5 m at the coastline as shown in Fig. 5 in Part I. All test results presented are along the line perpendicular to the coastline 100 km from the southern boundary. In all the tests, the sea state is represented by a continuous and steady swell system given by the spectrum shown in Fig. 6a in Part I. The swell condition is prescribed at every grid point at the open ocean boundary. The incoming swell system has relatively small angular and frequency distri-

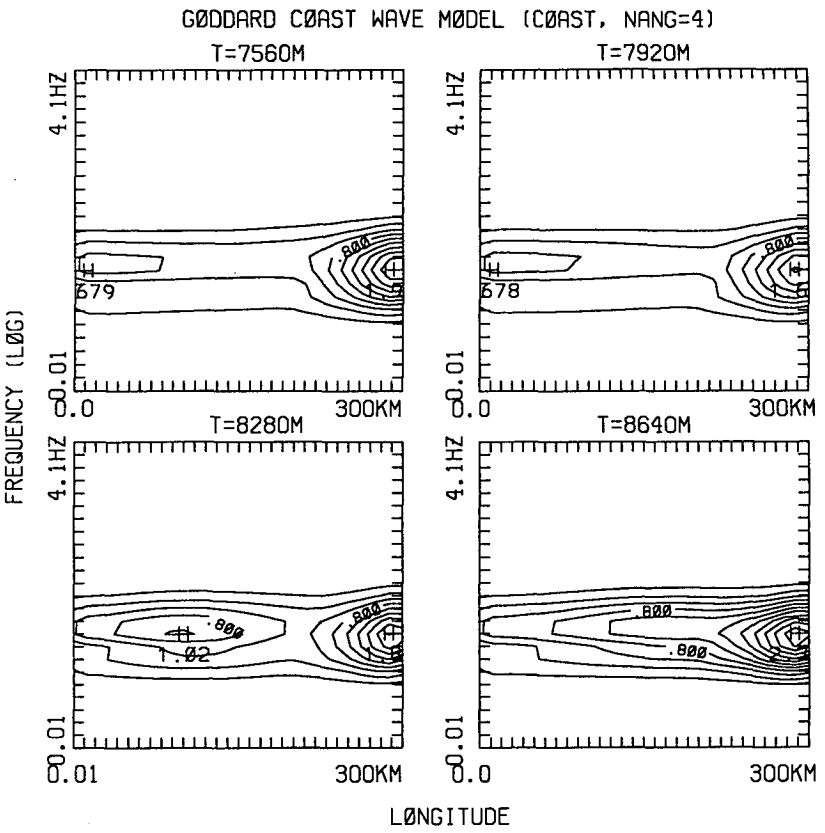

FIG. 5. Results for the coastal region with a periodic tidal current, case 3, from GCWAM for one tidal cycle (from 7560 min after the initiation of the test). To illustrate the effect of a nonlinear dispersion relationship, both linear and nonlinear dispersion relationships will be used in case 3. The linear dispersion is used in this case. (a) Wave energy in the direction number 4 (toward the east direction perpendicular to the coastline), (b) wave energy in the direction number 5, and (c) wave energy in the direction number 6.

bution ranges, with the maximum energy density propagating in direction number 6. For each test, the test area is calm initially. The swell system enters the test region from the open ocean side. To allow for the transient period with the highest frequency components to pass, the models are run for five days before test results are selected for detailed comparisons. All the computations for the GCWAM are performed in terms of action density as given in the model equation, but the results are presented for the energy density spectrum because energy is a more assessable quantity for comparisons.

For the coastal region, the grid mesh size $\Delta x = \Delta y = 12.5$ km, $\Delta\theta = \pi/6$, and $\Delta f = 0.1f$. The time step of the WAM is 5 min, but the time step of GCWAM is 10 min.

The specific cases considered are listed as follows: first, a coastal region without current; second, a coastal region with a steady shear current along the coastline flowing from south to north; third, a coastal region with an on- and-offshore tidal current of 24-h. period.

Other than the boundary on which the incoming swell condition is prescribed, all other boundaries are open; therefore, energy can flow through the boundary without any impedance even at the coastline. Granted that this open boundary condition at the coastline is artificial, we adopted it because our objective here is to test the propagation scheme only. The true dynamic consequence of the energy dissipation due to bottom friction and more realistic wave breaking from the depth limitations are deferred until the discussion of the source functions.

Because the full nonlinear dispersion relationship is derived based on perturbation analysis, its ordering and magnitude are all energy density related; therefore, we have to institute a check so that, as the water depth decreases, the increasing energy density does not cause the higher order terms to overpower the lower order ones. To guarantee this ordering, we impose a breaking criterion: The waves will break when $ak \geq 0.4$ in the computations. The amount of wave energy exceeding this limit will be set to zero. This criterion is a rather conservative one, for the Stokes limit puts ak very close to unity. In view of the laboratory and field observations as summarized by Huang et al. (1986), we feel this choice is justifiable.

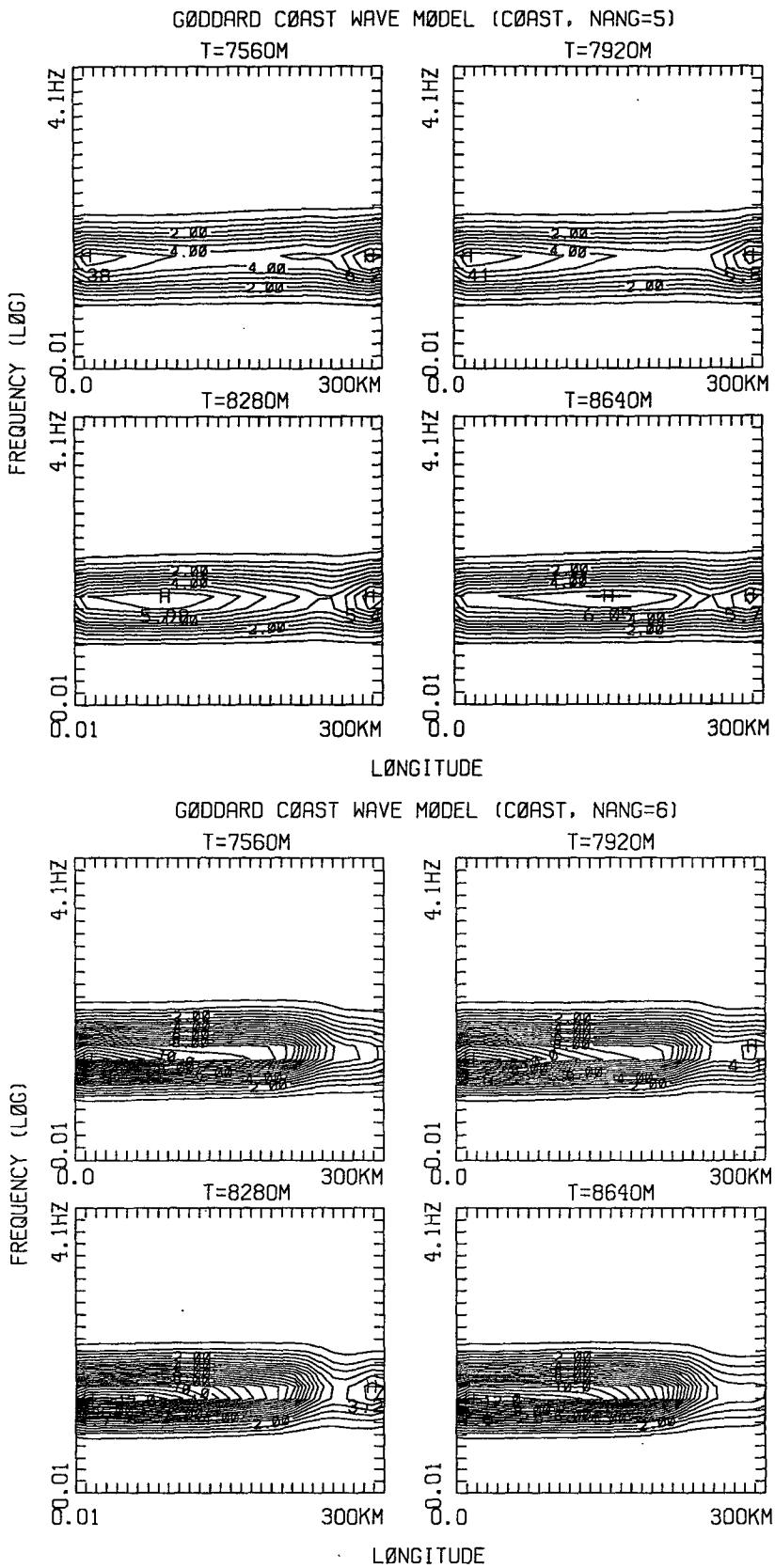

FIG. 5. (*Continued*)

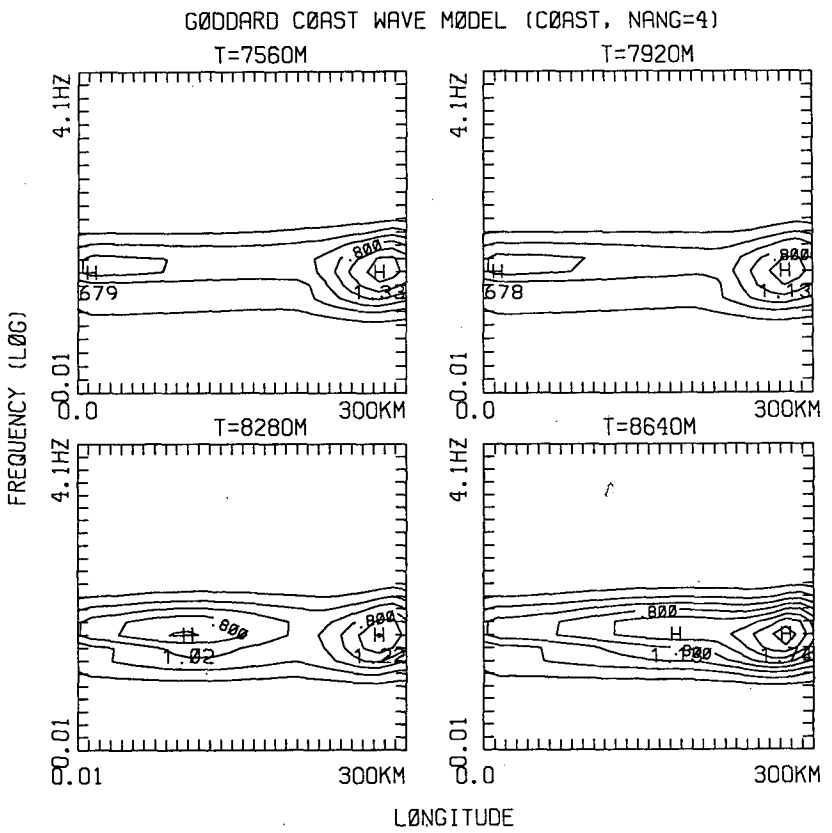

FIG. 6. Same conditions as for Fig. 5 except that a nonlinear dispersion relationship with a breaking criterion is used. Notice the slight frequency upshift of the energy near the coastline due to the finite amplitude effects in the dispersion relationship. (a) Wave energy in the direction number 4 (toward the east direction perpendicular to the coastline), (b) wave energy in the direction number 5, and (c) wave energy in the direction number 6.

Other values can be easily substituted in the future, if they prove to be more realistic.

a. Coastal region without current

This is the simplest condition; the results can serve as a reference to examine the variations of the more complicated conditions. We will run the WAM for this case only. The results would be identical for all the subsequent cases with various currents, because the version we have access to does not include the wave–current interaction or depth change as part of the model. Therefore, for the comparisons with the subsequent cases between GCWAM and WAM, we can only refer to the WAM results of this case.

Figures 2a–c show the numerical simulation of energy density spectrum by the WAM. Figure 2a represents the energy density in the direction number 4, perpendicular to the coastline toward the east; Fig. 2b in the direction number 5; and Fig. 2c in the direction number 6. In all these figures, the horizontal axis represents the west to east physical distance starting from the open ocean end, while the vertical axis represents the logarithm of frequency.

As expected, Figs. 2a–c show that the swell energy at any frequency remains constant along the propagation path, a consequence of energy transport without sources or sinks. These are state-of-the-art wave model results. Since the WAM does not include current effects, the results with currents will be identical to those presented here.

As a special test of the effects of different model equations, the GCWAM is used here with linear dispersion relation as in the WAM. Even with this simplification, the depth effects still become dominating. Energy pileup occurs as shown in the Figs. 3a–c, as predicted by the analytic results of Phillips (1977). Other than this expected energy pileup, there is an unexpected shift of energy toward low frequencies near the coastline in the energy propagation directions number 5 and 6. This shift can be explained by recalling the second term of Eq. (18). For the cases with no current, or steady-state current when $\vec{k}\cdot\vec{v} = 0$, c_ω depends only on

$$(\vec{c}_g + \vec{v})\cdot\nabla\sigma = \frac{\partial\sigma}{\partial d}(\vec{c}_g + \vec{v})\cdot\nabla d$$

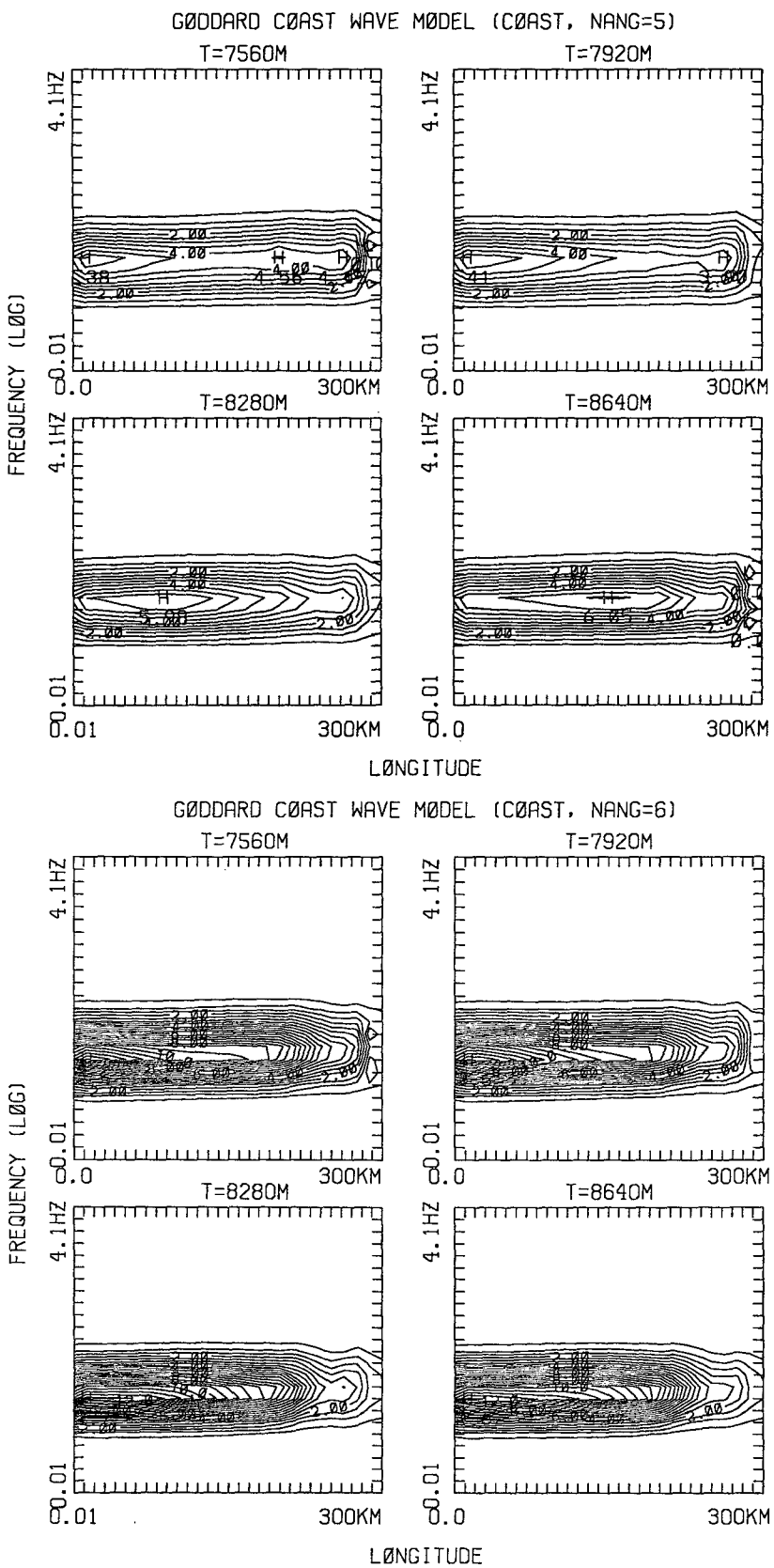

FIG. 6. (*Continued*)

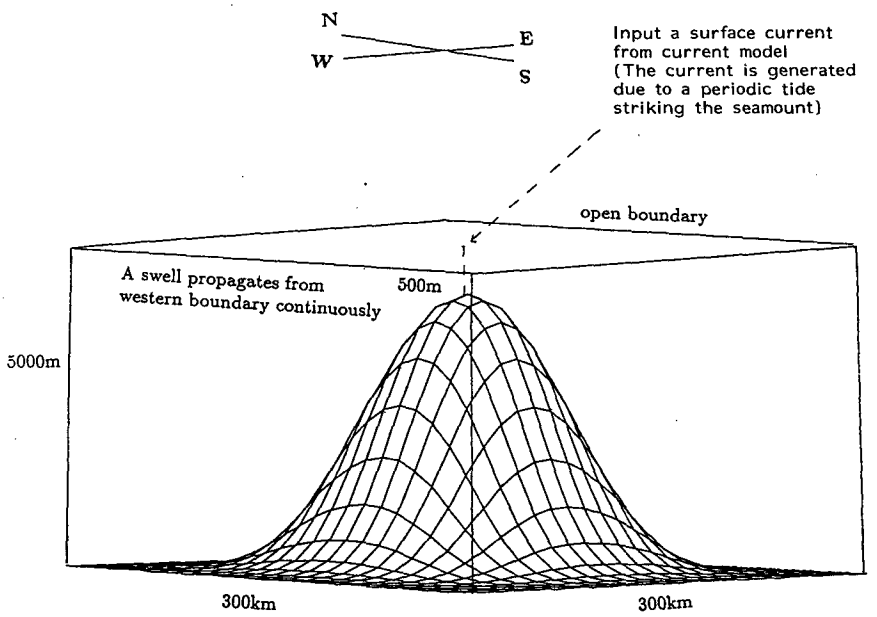

FIG. 7. A prospective view of the open ocean seamount region and the test condition (Experiment 4). The test region is a 300 km × 300 km box with open boundaries. The free tidal current is in the east–west direction at 0.2 m s^{-1}. The swell condition is the same as in the coastal cases.

since

$$\frac{\partial \sigma}{\partial d} = \frac{g[k \operatorname{sech}(kd)]^2}{2\sigma} > 0;$$

therefore, the sign of c_ω depends on $(\vec{c}_g + \vec{v})\cdot\nabla d$. When waves propagate into shallow water, c_ω becomes negative. The negative sign here contributes to the downshift of frequency. This term is not included in the WAM, which is one reason why it cannot fully model coastal regions.

b. *Coastal region with a steady nonuniform current*

Next, we will study the same coastal region with the additional steady but nonhomogeneous shear current seen in case 2 of Fig. 1. The current flows from south to north along the y direction with its current speed increasing linearly from 0.2 m s^{-1} in the open ocean to 1.0 m s^{-1} at the coastline. Since the WAM contains no provision for current, its results would be identical to those given in Figs. 2a–c. To test the effect of the shear current, we ran the GCWAM with the linear dispersion relationship as in the case with no current, and found the main effect was to cause additional energy refraction, with the energy density in all directions enhanced. As expected, the smallest variation is in the direction perpendicular to the coast, along which the linear model will give no change at all. As the wave propagation direction changes, the variations becomes more noticeable. For the sake of space, the results are not shown here. Instead, the results using GCWAM with the full nonlinear dispersion relationship are given in Figs. 4a–c for wave energy in the direction number 4, 5, and 6 respectively. Here the breaking criterion together with the nonlinear dispersion relationship causes the energy density to change in more than one way. The trace of the energy enhancement due to the shear current can still be seen 100 km offshore in the direction number 4 and 5, where the maximum energy density is higher than the corresponding cases with no current. But at the coastline, the breaking criterion has exacted a much heavier toll on the energy density. It has eliminated energy pileup due to the depth effect. The energy is no longer the greatest at the coastline.

The shear considered here is a simple one. When the shear current meanders, additional energy refraction will result through focusing and defocusing (Liu et al. 1989). Also Holthuijsen and Tolman (1991) pointed out that observations from ships, aircraft, and spacecraft showed that ocean waves approaching the east coast of the United States are affected by the Gulf Stream. Other studies by Dingemans et al. (1986), Holthuijsen and Tolman (1991), and Sakai et al. (1983) have all indicated the effects of either current or the combination of current and depth on the wave field. The currents tend to create a confused sea state, often with local wave energy higher than incoming waves. Similar observations have been made off the coast of South Africa, Japan, and California. The results in Fig. 4 are consistent with those observations in indicating the modulations caused by the shear current.

In the presence of steady state current, there is additional reason why the energy shifts to lower frequencies near the coastline when $\vec{k}\cdot\vec{v} \neq 0$. Recall the third term of the Eq. (18)

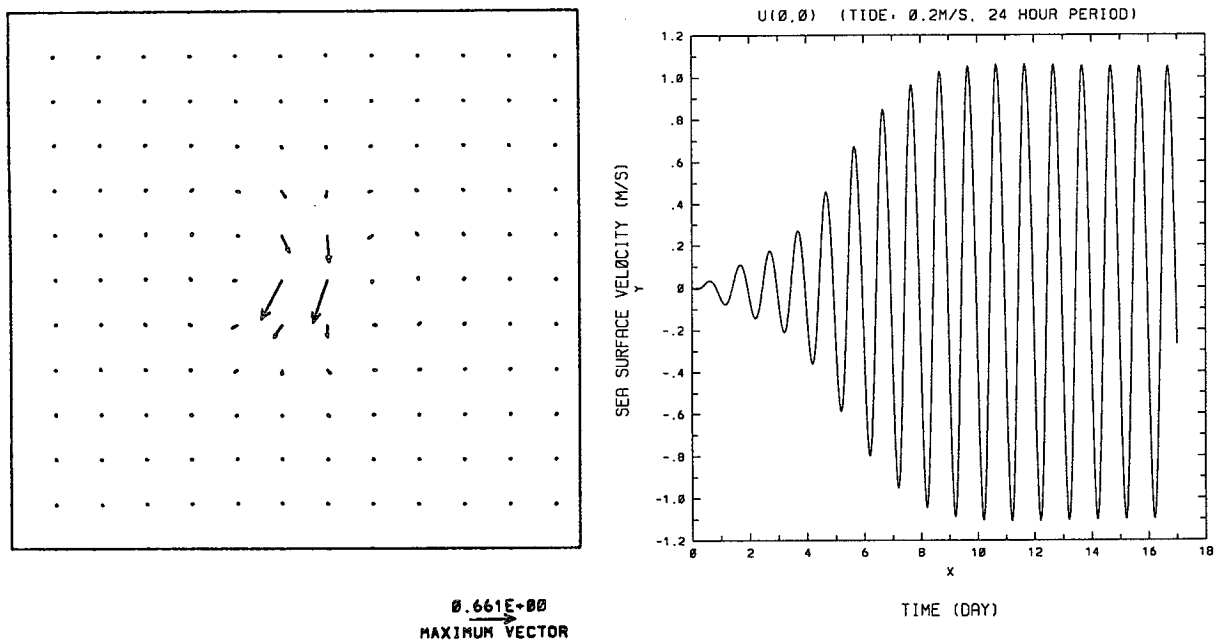

FIG. 8. The numerical simulation of the ocean surface velocity over the seamount. The resonant interaction between the tidal current and the local internal wave frequency produces a surface current much stronger than the free tidal current. (a) The spatial distribution of the surface velocity over the seamount. (b) The time series of the horizontal velocity component over the seamount.

$$(\vec{c}_g + \vec{v})\cdot\nabla(\vec{k}\cdot\vec{v}) = \left[\frac{\partial\vec{k}\cdot\vec{v}}{\partial d}\right](\vec{c}_g + \vec{v})\cdot\nabla d.$$

Since $\partial k_y v/\partial d < 0$ and $\vec{k}\cdot\vec{v} = -k_y v$ in this case, we must have $\partial\vec{k}\cdot\vec{v}/\partial d = -\partial k_y v/\partial d > 0$. This condition again causes $c_\omega < 0$ when the waves propagate into shallow water.

c. *Coastal region with a periodic tidal current*

Next, we present the results for case 3 with an additional 24-h period tidal current in the on–offshore direction. The tidal current increases along the west-to-east direction from 0.2 m s^{-1} at the open ocean to 1 m s^{-1} at the coastline. This is the first case in which we have a time-dependent current as well as topographic features; therefore, we will present more detailed comparisons between the GCWAM with linear and nonlinear dispersion relationships.

Figures 5a–c show the numerical simulation results for the energy spectral distribution in GCWAM with a linear dispersion relationship for the direction number 4, 5, and 6 respectively. Figures 6a–c show the corresponding results with a nonlinear dispersion relationship given. As the breaking criterion has only been imposed on the nonlinear dispersion case, the effects of breaking appear only in the nonlinear cases.

The effects of currents in these cases are drastic: First, the energy density fluctuates with the period of the tidal current. As shown in Fig. 5a, the maximum values at the coastline vary from 1.6 to 2.3 m^2 Hz, depending on the tidal cycle. In both Figs. 5a and 5b, the locations of the maximum values move with the tidal cycle; however, in Fig. 5c, the maximum energy density regions always remain in the deep ocean and only extend their fronts with the tidal cycle.

When comparing the cases with linear and nonlinear kinematics, we found that the main nonlinear effect is to eliminate the energy pileup at the coastline as in the previous case. This is more related to the imposed breaking criterion than to the dispersion relationship. The lack of breaking is also the main reason why the linear model shows more total wave energy than the nonlinear model.

Nonlinear effects, as expected, should be weak at the open ocean end as the results indeed show. They should be stronger near the coastline, but, unfortunately, the breaking criterion has clouded this issue. Yet weaker effect can be discerned: the nonlinear dispersion does cause more energy to approach, but not reach, the coastline as shown in Fig. 5c versus Fig. 6c. This, however, is only a relative effect. Other studies should be devised to delineate this effect more clearly.

d. *Deep ocean waves over a seamount with a tidal current*

The final case we studied is a deep ocean with a seamount and unsteady tidal current. The region modeled is a 300 km × 300 km box with open boundaries. A bell-shaped seamount 4500 m in height and 40 km in radius at half-height is located in the center of the area under a 5000-m deep ocean. A perspective view

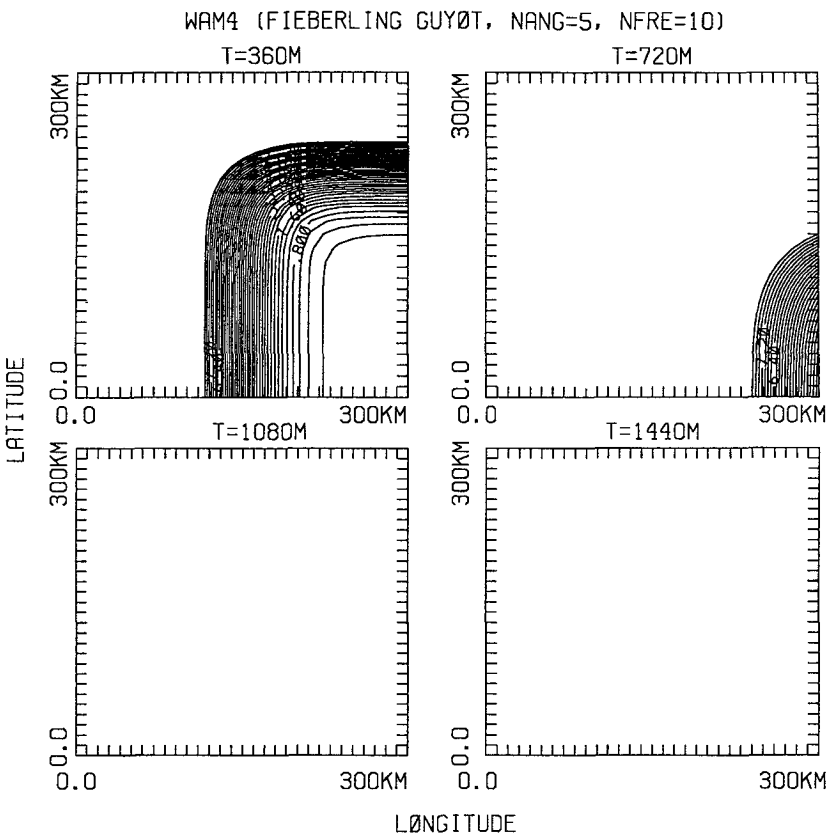

FIG. 9. Comparisons between the energy density distributions produced by the WAM and GCWAM, for a frequency of 0.1037 Hz in the direction number 5. (a) WAM results during the transient stage; the wave front propagates without any tidal current effects. By the time the wave front passes through the test section, the wave energy contour becomes uniform. (b) GCWAM results during the same period as in (a); the effects of the tidal current effects are clearly visible. (c) GCWAM results through a whole tidal cycle. The current wave interactions cause the sea state to vary with the tidal cycle, a phenomenon documented by SAR observations.

of the test condition is given in Fig. 7. This bottom topography is similar to that of Fieberling Guyot in the Pacific Ocean, which has been studied extensively by Etkin et XIV al. (1991).

We assume a 24-h period 0.2 m s^{-1} free tidal current flowing in the east–west direction covering the entire ocean. The tidal current near the seamount will be modified as shown by Haidvogel et al. (1993). The sea state is represented by the same swell spectrum used in the coastal tests. Following an initial calm state, a continuous and steady swell system will enter the test area from the north and the west boundaries at $t = 0$. Then, the swell conditions will be prescribed at each point on these boundaries continuously and steadily.

A numerical simulation of the resonantly trapped tidal energy has been modeled based on a modified σ coordinate coastal model by Haidvogel et al. (1993). For the present numerical simulation, we chose the Burger number (Bu = Nh/fw) = 1.125, where N is a Brunt–Väisälä frequency, h is the height of the seamount, w is the width of the seamount, and f is the inertial frequency. This Burger number is chosen to simulate the resonant case when the free wave frequency of the Fieberling Guyot is close to the forcing frequency. A strong nonlinear thermocline near the sea surface is adopted based on observational data, presenting an optimum condition for a bottom-trapped wave near an isolated seamount to also occur near the sea surface. The resonant oscillation will produce a strong current field as discussed by Haidvogel et al. (1993). Figure 8a shows a typical sea surface current distribution based on the model results, where the tidal current changes not only in magnitude but also direction. The velocity values over the seamount are much greater than the free tidal velocity elsewhere. Figure 8b shows a time series of sea surface horizontal velocity in the x direction over the top of the seamount. The surface velocity oscillates with a 24-h period, which is similar to the tidal forcing. The absolute maximum velocity over the whole tidal period can be as high as 1.05 m s^{-1}, which is about five times greater than the free tidal current. The model-calculated sea state for the fre-

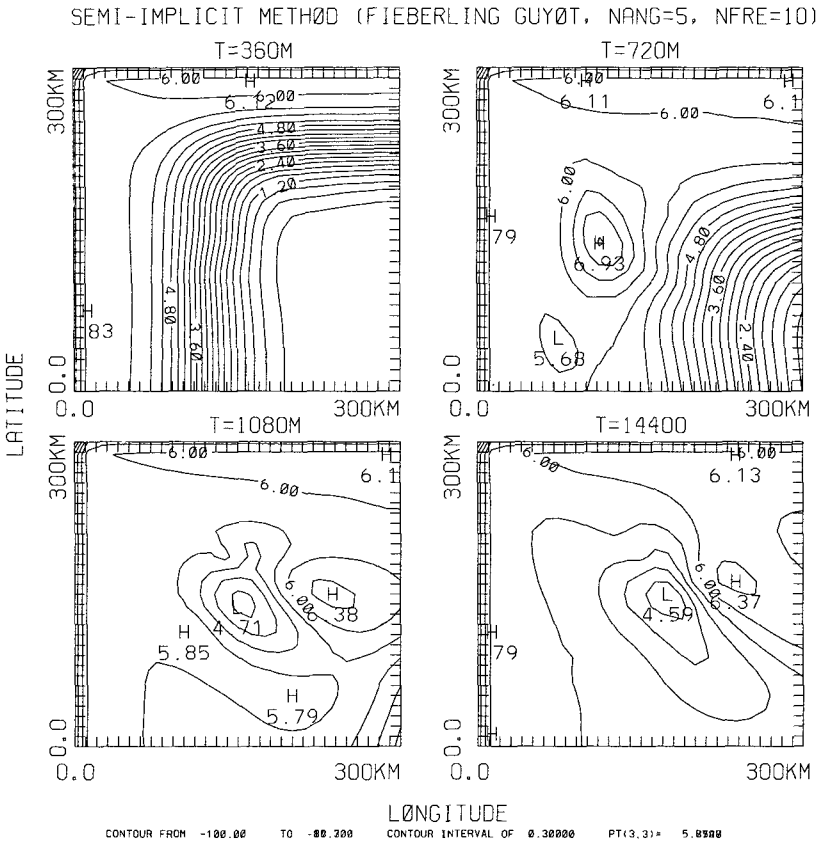

FIG. 9. (*Continued*)

quency component at 0.1037 Hz along the direction number 5 covering a whole tidal period is shown in Figs. 9a–c.

First, we will examine WAM results during the initial transient stage in Fig. 9a. As we turn on the swell condition, the waves start to enter the test region from the north and the west boundaries. At a time 360 minutes after the initiation, the swell front is clearly visible. By the time of 720 minutes, the swell front has almost passed through the test region. Subsequently, the sea state becomes uniform as assumed. Since the WAM does not include current effects, it does not predict any signature of the seamount in the sea state at the surface.

The results from the GCWAM are quite different. Even during the transient state as the wave front propagates through the test region, the influence of the tidal current is visible as shown in Fig. 9b. Again, by 1080 minutes after the initiation of the model run, the initial swell front structure has passed through totally. Figure 9c shows the sea state during a whole tidal cycle after the wave front has long passed through the test region. The uniform sea state predicted by the WAM now becomes highly variable due to the effects of the tidal current. The regions with the maximum variations also move with the tidal cycle. This pattern is in qualitative agreement with observations from Spaceborne Synthetic Aperture Radar (see, for example, Etkin et XIV al. 1991). To make quantitative comparisons, we have to extend our model to a higher cut-off frequency than is used here, so that the Bragg component for the SAR will either be included, or the indirect wave–wave interactions between the long-wave and the short-wave components will be included. However, either case is beyond the scope of the present paper.

4. Summary

Based on our comparisons, we conclude that the GCWAM will produce more realistic results than the WAM due to the improved numerics and kinematics. Even for the case of a flat bottom of finite depth, the numerical dispersion and the dissipation in the WAM will annihilate energy computationally as discussed in Part I. Additional differences between the two models becomes obvious whenever there are ambient currents and depth changes. In the coastal region, tidal currents and depth changes are the norm rather than the exception; therefore, any model that is to be applied to the coastal region should definitely include these factors. The GCWAM is based on the action conservation law, which enables us to include the current effects readily. It also includes a more detailed computation of the dispersion effects due to an unsteady current and bottom topography.

From the model results, we can see that there are significant differences between the WAM and GCWAM when there is a steady or unsteady current, or when a rough bottom topography and shallow waters are included. Comparison with the analytical results for simpler cases convinces us that the new model represents the kinematics more realistically. Over the deep ocean, if there are rough topographic features such as an isolated seamount, the new model will also offer more realistic answers. Based on these studies, we conclude that the GCWAM offers a better alternative than the current WAM model for coastal regions.

Acknowledgments. We would like to thank Drs. H. S. Chen of NMC/NOAA; Erik Mollo-Christensen of Lexington, MA; Steven R. Long of NASA/WFF; and Professor O. M. Phillips and Mr. J. Hansen of the Johns Hopkins University for their discussions and suggestions. This research has been supported by ONR Coastal and Physical Oceanography Programs, and the NASA Physical Oceanography Program.

REFERENCES

Bretherton, F. P., and C. J. R. Garrett, 1968: Wave trains in inhomogeneous moving media. *Proc. Roy. Soc. London,* **A302,** 529–554.

Dingemans, M. W., M. J. F. Stive, J. Bosma, H. J. de Vriend, and J. A. Vogel, 1986: Directional near-shore wave propagation and induced currents. *Proc. 20th Int. Conf. Coast Engineering,* Taipei, Taiwan, ASCE, 1092–1106.

Etkin, V. S., and Coauthors, 1991: Radiohydrophysical aerospace research of ocean. Academy of Sciences USSR, Space Research Institute Pub. 1749, 83 pp.

Günther, H., S. Hasselmann, and P. A. E. M. Janssen, 1993: The WAM model cycle 4. DKRZ WAM Model Documentation, 91 pp.

Haidvogel, D. B., A. Beckmann, D. C. Chapman, and R. Q. Lin, 1993: Numerical simulation of flow around a tall isolated seamount. Part II: Resonant generation of trapped waves. *J. Phys. Oceanogr.,* **23,** 2373–2391.

Holthuijsen, L. H., and H. L. Tolman, 1991: Effects of the Gulf Stream on ocean waves. *J. Geophys. Res.,* **96,** 12 755–12 771.

Huang, N. E., L. F. Bliven, S. R. Long, and C. C. Tung, 1986: An analytic model for oceanic whitecap coverage. *J. Phys. Oceanogr.,* **16,** 1597–1604.

Infeld, E., and G. Rowlands, 1990: *Nonlinear Waves, Solitons and Chaos.* Cambridge University Press, 423 pp.

Lin, R. Q., and N. E. Huang, 1996: The Goddard Coastal Wave Model. Part I: Numerical method. *J. Phys. Oceanogr.,* **26,** 833–847.

Liu, A. K., F. C. Jackson, E. J. Walsh, and C. Y. Peng, 1989: A case study of wave–current interaction near an ocean front. *J. Geophys. Res.,* **94,** 189–200.

McLean, J. W., 1982: Instabilities of finite-amplitude gravity waves on water of finite depth. *J. Fluid Mech.,* **114,** 331–341.

Phillips, O. M., 1977: *Dynamics of the Upper Ocean.* 2d ed. Cambridge University Press, 336 pp.

Sakai, T., M. Koseki, and Y. Iwagaki, 1983: Irregular wave refraction due to current. *J. Fluid Mech.,* **109,** 1203–1215.

Tolman, H. L., 1991: A third-generation model for wind waves on slowly varying, unsteady, and inhomogeneous depth and currents. *J. Phys. Oceanogr.,* **21,** 782–797.

——, 1992: Effects of numerics on the physics in the third-generation wind-wave model. *J. Phys. Oceanogr.,* **22,** 1095–1111.

WAMDI Group, 1988: The WAM model—A third generation ocean wave prediction mode. *J. Phys. Oceanogr.,* **18,** 1775–1810.

Whitham, G. B., 1974: *Linear and Nonlinear Waves.* John Wiley and Sons, 636 pp.

Yuen, H. C., and B. M. Lake, 1982: Nonlinear dynamics of deep-water gravity waves. *Adv. Appl. Mech.,* **22,** 69–229.